Theoretical and Applied Climatology (2024) 155:1493–1506
https://doi.org/10.1007/s00704-023-04704-w

RESEARCH

Climatology and pre-convection environmental conditions of dry and wet thunderstorm high winds over eastern China

Fuyou Tian[1] · Xiaoling Zhang[1] · Jianhua Sun[2] · Kun Xia[3] · Shan Hua[1] · Qian Wei[2] · Lulin Xue[4] · Bo Yang[1]

Received: 4 March 2023 / Accepted: 11 October 2023 / Published online: 17 October 2023

Abstract

Thunderstorm high wind (THW) is defined as a kind of convective weather phenomenon with a maximum wind gust speed not less than 17.2 $m{\cdot}s^{-1}$ over China. It is a sudden, damaging, but common convective weather phenomenon during the warm seasons of China. By adopting a kernel density estimation (KDE) for the THWs during warm seasons (March–September) of 2010–2019 over eastern China and the European Centre for Medium-Range Weather Forecasts Reanalysis v5 (ERA5) dataset, the dry and wet THWs usually with different mechanisms are objectively obtained, and climatology and pre-convection environmental conditions investigated. KDE shows the total precipitable water (TPW) of 38 mm can be used as the threshold for distinguishing dry THWs from wet ones. Dry THWs mainly concentrate in North China and Yunnan province, while wet ones mainly concentrate in South China. West of Hebei province has high frequencies for both dry and wet THWs. A comparison of pre-convection environmental conditions shows dry THWs mainly occur under environmental conditions with lower saturation at both the middle-lower and upper layers, while wet ones usually have relatively lower saturation at the middle-lower layers. The instability of wet THWs can be well characterized by the most unstable lifted index (MULI) and most unstable convective available potential energy (MUCAPE), while dry ones can be well depicted by the lower 500 hPa temperature caused higher temperature difference (DT85) or temperature lapse rate (TLR85) between 850 and 500 hPa. The 0–6-km vertical wind shear (SHR_6) can distinguish dry THWs from wet ones better than SHR_1. The typical difference can be comprehensively revealed by the representative soundings. The results provide objective references for understanding and forecasting THWs under dry and wet environmental conditions.

Keywords Thunderstorm high winds (THWs) · Pre-convection environmental conditions · Total precipitable water (TPW) · Kernel density estimation (KDE) · Climatology of dry/wet THWs

1 Introduction

Thunderstorm high wind (THW) is a kind of suddenly happened destructive convective weather phenomenon (Smith et al. 2013; Yang et al. 2017a; Pacey et al. 2021). China usually suffers from THWs during the warm seasons. Widespread severe THWs swept across the east of He'nan province and surrounding areas in the afternoon of June 3, 2009, and caused severe damage (Wang et al. 2012). On June 1, 2016, the tourist ship "Oriental Star" sailing on the Yangtze River was blown down by a sudden THW event with a maximum wind speed of at least 31.0 $m{\cdot}s^{-1}$ (Meng et al. 2016; Zheng et al. 2016), and 442 people were killed.

THWs are common in tropical and subtropical areas but have different definitions in different countries and regions. A study focused on convective wind gusts occurring in Germany defines those not less than 18.0 $m{\cdot}s^{-1}$ as severe

✉ Fuyou Tian
tianfy@cma.gov.cn

1 National Meteorological Center, China Meteorological Administration, Beijing 100081, China

2 Key Laboratory of Cloud-Precipitation Physics and Severe Storms (LACS), Institute of Atmospheric Physics, Chinese Academy of Sciences (IAP/CAS), Beijing 100029, China

3 State Key Laboratory of Numerical Modeling for Atmospheric Sciences and Geophysical Fluid Dynamics (LASG), Institute of Atmospheric Physics, Chinese Academy of Sciences (IAP/CAS), Beijing 100029, China

4 Research Applications Laboratory (RAL), National Center for Atmospheric Research (NCAR), Boulder, CO 80307, USA

wind events (Mohr et al. 2017). Convective wind gusts not less than 25.0 $m{\cdot}s^{-1}$ are considered severe ones in the USA (Doswell 2001), Australia (Brown and Dowdy 2021), and some European studies (Pacey et al. 2021). The convective gales exceeding 17.2 $m{\cdot}s^{-1}$ are defined as THWs by the National Meteorological Center (NMC), China Meteorological Administration (CMA).

THWs are usually produced by the mesoscale convective system (MCS) with different organizational modes. The organizational modes of MCS and related convective phenomena, the classification, and background conditions based on radar echoes are fully studied (Bluestein and Jain 1985; Parker and Johnson 2000; Jirak et al. 2003). All the bow echoes (Fujita 1978; Przybylinski 1995; Weisman 2001; Klimowski et al. 2004), squall lines (Smull and Houze 1985; Parker and Johnson 2000), and super-cells (Moller et al. 1994) can produce THWs. In the USA, non-tornadic severe wind events are caused mainly by bow echoes, squall lines, and broken lines (Klimowski et al. 2003; Duda and Gallus 2010; Schoen and Ashley 2011; Smith et al. 2012, 2013).

The understanding of the mechanisms of THWs is still under development. Fujita (1978) documented that THWs are formed by descending to the ground of the mid-level inflow behind the bow echo. Houze et al. (1989) proposed the conceptual model of a squall line with a trailing stratiform area. There are intense localized updrafts and downdrafts within the convective region. Wheatley et al. (2006) confirmed the close relationships between mid-level inflow and surface-damaging wind with radar and ground surveys of wind damage. Numerical simulation and radar analysis studies in recent years show that low-level meso-γ-scale vortices within bow echoes and squall lines are the producers of the primary damage swath (Trapp and Weisman 2003; Atkins et al. 2005). The formation of low-level mesovortices and the cause of surface strong damaging wind are also studied (Wakimoto et al. 2006a, b; Atkins and Laurent 2009a, b). Xu et al. (2015) show that the mesovortices originate from the tilting of near-surface horizontal vorticity are mainly created via surface friction. The dominating organizational modes associated with THW may change with geography. For instance, severe gusts caused by quasi-linear convective systems are most frequent in the plains and the Midwest regions, whereas severe gusts with disorganized storms are mainly in the plains and the intermountain West (Gallus et al. 2008; Smith et al. 2013).

Environmental conditions and mesoscale schemes might be different favoring different THW intensities. Wakimoto (1985) concluded that the presence of moisture at mid-levels is the main feature, and the evaporation of precipitation during the descent below the cloud base is the main cause of dry THWs. Atkins and Wakimoto (1991) summarized that the moisture for wet microbursts is present at low level, and capped by a mid-level dry layer. However, Kuchera and Parker (2006) found that dry air entrainment in the mid-levels is not uniquely associated with damaging winds. James et al. (2006) documented that the hook echo is sensitive to environmental moisture content and cold pool strength, and found that they are strongly sensitive to the ambient water vapor mixing ratio. Roberts and Wilson (1989) and Wolfson et al. (1990) found that cold pools are often formed by the relatively large-scale gust front under wet environments. However, no clear definition on types of environments such as wet or dry is found.

There are studies on THWs carried out in China. Fan and Yu (2013) found that the environmental differences between THWs and hails (maximum diameter greater than 5 mm) were not significant, but they were significantly different from those of short-duration heavy rainfall (hourly rainfall greater than 20 $mm{\cdot}h^{-1}$). A study on stronger THWs (≥ 25 $m{\cdot}s^{-1}$) carried out by Fei et al. (2016) shows the obvious dry intrusions in the middle troposphere were notable. Ma et al. (2019) studied extreme THWs (≥ 30 $m{\cdot}s^{-1}$) in China and pointed out that the main feature is also the existence of obvious dry intrusion. Yang et al. (2017b) and Ma et al. (2021) analyzed the THWs environment in South China and North China, respectively, but did not distinguish between wet and dry environments. Meng et al. (2013) investigated the general features of squall lines in East China and found that the squall lines tend to form in an environment with more moist and weaker vertical shear relative to their US counterparts. Sun et al. (2014) and Zheng and Sun (2016) found that the organization modes and intensities of MCSs can be significantly affected by vertical wind shear and vertical distribution of moisture. A 50 mm of total precipitable water (TPW) was arbitrarily taken by Zheng and Sun (2013) as the threshold for distinguishing dry and wet MCS environments. Tian et al. (2022) indicate that there is seemingly a significant TPW threshold for distinguishing the dry and wet THW environments (shortly for dry THWs and wet THWs) but much smaller than 50 mm.

The environmental conditions and concerns about forecasting dry and wet THWs are very different (Wakimoto 1985; Atkins and Wakimoto 1991). With a newly available THWs observational dataset, the TPW threshold for distinguishing dry and wet THWs is objectively determined, and general climatological characteristics and pre-convection environmental conditions are investigated in this study.

2 Datasets and quality control

2.1 Observational data source and quality control

The 3-hourly severe weather reports (SWRs), hourly routine observations at surface weather stations, the cloud-to-ground lightning observation data during 2010 and 2019, as well

as European Centre for Medium-Range Weather Forecasts (ECMWF) Reanalysis v5 (ERA5) hourly estimates (Hersbach et al. 2020) of atmospheric variables are used in this study.

The severe wind event observations with a time interval of 3 h were obtained from the severe weather reports (SWRs). In each file, all severe weather events that occurred in the 3-h period were recorded with station ID, location (longitude and latitude), exact time (hour and minute), weather phenomena, and other information. THWs are obtained based on the following quality control processes. Firstly, cloud-to-ground lightning data from the China Lightning Detection Network (CLDN) were used to remove severe wind events associated with weak thunderstorms or without thunderstorms by comparing the intensities of cloud-to-ground lightning between each severe wind event and the climatic background in the same month (Yang et al. 2017a). Secondly, the influences of typhoons are excluded by investigating whether the distance of a THW from the center of a typhoon is less than 800 km.

Additional quality control processes are executed as there are still some records that could not be determined to be true or not. The stations located at prominent highlands, canyons, islands, offshore, and coastal regions are excluded (Fig. 1a). The stations located at prominent highlands, canyons, and islands are excluded directly by checking the altitudes and surrounding geographical conditions. For the offshore and coastal stations, the total number of THWs is compared with the nearest land station. The offshore or coastal station is excluded if the total THWs is three times more. The stations located in the Northwest or with an altitude greater than 2000 m are excluded as severe damaging THW events are mainly reported over the low-altitude areas of central and eastern China (Wang et al.

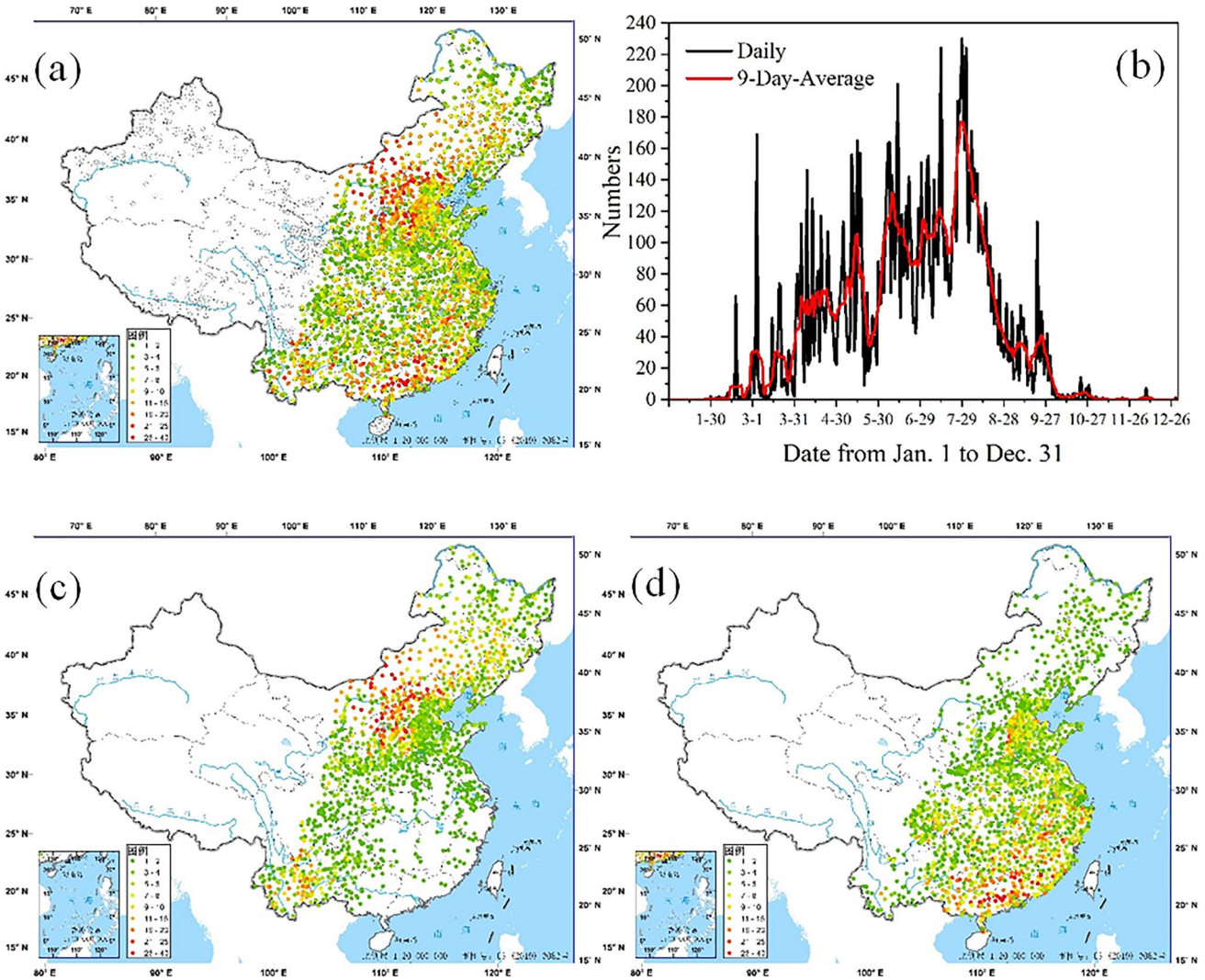

Fig. 1 The spatial distribution of total dry and wet THWs and the yearly variation of total THWs. The stations excluded in this study are given as black circles. **a** The spatial distribution of all studied THWs. **b** The yearly cycle of total THWs. **c** The spatial distribution of dry THWs. **d** The spatial distribution of wet THWs

2012; Meng et al. 2016; Zheng et al. 2016). Finally, a total of 2142 stations (Fig. 1a, colored dots) among 2710 stations with the data during 2010 and 2019 are investigated.

2.2 Environmental parameters

The sounding observations were too coarse to represent the environments of THWs. Instead, the high-resolution ERA5 data (Hersbach et al. 2020) is used. The horizontal grid spacing is 0.25°, and there are 28 vertical levels, consisting of one surface level and 27 pressure levels from 1000 to 100 hPa. The data used in this study cover the 10 years from 2010 to 2019. All the basic parameters are obtained directly with the ERA5 data while some other quantities are additionally calculated. The closest hour before the exact time of each of the THW is obtained and used for the pre-convection environment of THWs. The high quality of the ERA5 data ensures the credibility of results (Zhang et al. 2019; Hersbach et al. 2020; Wang et al. 2023).

The studied parameters (Table 1) are selected according to known studies. TPW can help distinguish between different types of convective weather phenomena (Ma et al. 2021; Tian et al. 2022). Dry intrusion and degrees of atmospheric saturation characterized by relative humidity are important for THWs (Fei et al. 2016; Ma et al. 2019). The most unstable layer convective available potential energy (MUCAPE) rather than the surface-based layer CAPE (SBCAPE) is a commonly used physical quantity characterizing the strength of conditional instability. The most unstable lift index (MULI) is also used to characterize the strength of conditional instability (Galway 1956) and is sometimes a better indicator than MUCAPE (Tian et al. 2015a, 2015b). The temperature difference between 850 and 500 hPa (DT85) and the temperature lapse rate (TLR85) are common indicators of atmospheric stability status (Bryan and Fritsch 2000; Nakamura 2011). The temperatures of 500 hPa (T_{500}) and 850 hPa (T_{850}) are also analyzed to understand the high DT85 and TLR85. The low-level divergence of 925 hPa (DIV_{925}) and 850 hPa (DIV_{850}) characterizes the strength of low-layer dynamic lifting conditions (Tian et al. 2015a). Vertical wind shears are important factors of organized convection (Wang et al. 2009; Weisman and Klemp 1982). The lifting condensation level (LCL) is usually used as an estimate of the height of the cloud base.

3 General features of THWs

The regional distribution and annual variation characteristics of THWs are clear. The spatial distribution of total THWs shows two significant high-frequency areas (Fig. 1a): the North China and the South China. The maximum numbers of THWs over both the two high-frequency areas are high up to about 40 times. The scope with high THWs over the North China area is much wider than that over the South China high-frequency area. Shanxi, Hebei, and the center of Inner Mongolia are all covered by the North China high-frequency area. East of Guangxi, Guangdong, and south Hu'nan is the main coverage of the South China high-frequency area.

The annual variation of THWs has three main peak stages (Fig. 1b) as the running 9-day average number shows. The first peak stage appears in April–May. The number of daily THWs increases from about 20 to about 60. Then it quickly drops to about 40 at the end of May. But then the number of daily THWs increases sharply to about 100, the second peak. And then increases to about 180, the last peak at the end of July. The maximum daily THWs number is high up to about 220 occurred in the third peak. The moving forward of the three main growth stages of THWs numbers is in good consistent with the advance and retreat of subtropical high and the rainy seasons (Tao 1980). Though the growth of THWs is gradual, the decline is fast. Except for a small peak at the end of September, the average daily number of THWs drops quickly. Only a few THWs are reported after October 1. According to the annual variation, the THWs between March 1 and September 30 are finally used in this study, and the total sample size is about 18,000.

Table 1 List of studied parameters

Abbreviation	Parameter description	Unit	Others
TPW	Total precipitable water	mm	
RH	Relative humidity	%	200, 300, 500, 700, 850, and 1000 hPa
MULI	Most unstable lifted index	°C	Galway (1956)
MUCAPE	Most unstable convective available potential energy	J kg^{-1}	Moncrieff and Miller (1976)
DT85	850 and 500 hPa temperature difference	°C	
TLR85	850 and 500 hPa temperature lapse rate	°C km^{-1}	
T	Temperature	°C	500 and 850 hPa
DIV	Divergence	s^{-1}	850 and 925 hPa
SHR	Vertical wind shear	m s^{-1}	0 ~ 1 km, 0 ~ 3 km, and 0 ~ 6 km
LCL	Lifting condensation level	m	

4 Division of dry and wet THWs

Studies show that the scatter plots of parameters for THWs have two highly TPW-related kernel density estimation (KDE) centers overlapped with that for short-duration heavy rainfall and hail, respectively (Tian et al. 2022). The characteristic is still recognizable (Fig. 2) with the datasets used in this study.

TPW plays an important role in the division of dry and wet THWs environmental patterns. There are two high KDE centers in the TPW-MULI (Fig. 2a) and TPW-SHR6 (Fig. 2b). The contour lines of 0.05 mm·°C distinguish the two KDE centers significantly with the maximum KDE high up to 0.07 mm·°C. The TPW threshold distinguishes the two high KDE areas is about 38 mm. The responsible TPW for the two high KDE centers of TPW-MULI are around 20 and 50 mm. The characteristic is still clearly displayed in the TPW-SHR6 (Fig. 2b). The TPW corresponding to the two high KDE areas in TPW-SHR6 are still around 20 mm and 50 mm (Fig. 2b), but the central values of the two high-probability density regions corresponding to them are 0.02 mm·m·s^{-1}. The TPW-SHR6 plots are more scattered than those for TPW-MULI. The TPW threshold is also around 38 mm. However, there is only one single high KDE center in the MULI-SHR6 (Fig. 2c). It is the TPW that determines the two high KDE areas. THWs appearing in environments with a TPW less than 38 mm can be considered dry ones, while the others considered wet ones. However, the threshold is much smaller than that used by Zheng and Sun (2013). With this division, the sizes of dry and wet environmental THWs are about 9500 and 8200, respectively.

5 Characteristics of dry and wet THWs and their environmental conditions

5.1 Characteristics of dry and wet THWs

The THWs are divided into dry and wet ones with the TPW of 38 mm. Results show the components of the two high-frequency areas displayed by total THWs are very different (Fig. 1). The North China high-frequency area is mainly composed of dry THWs (Fig. 1c) while the South China high-frequency area is almost composed of wet THWs (Fig. 1d). Yunnan province, located in southwest China, is mainly composed of dry THWs. Central Fujian, southern and central Jiangxi, can be regarded as the extension of the high-incidence area of wet THWs. There are also a certain number of wet THWs in North China. Only a few THWs over Inner Mongolia are wet while only a few dry THWs are reported in central and South China. West of Hebei province has high frequencies for both dry and wet THWs.

There are also significant differences in the annual cycle of dry and wet THWs but with similar daily cycle

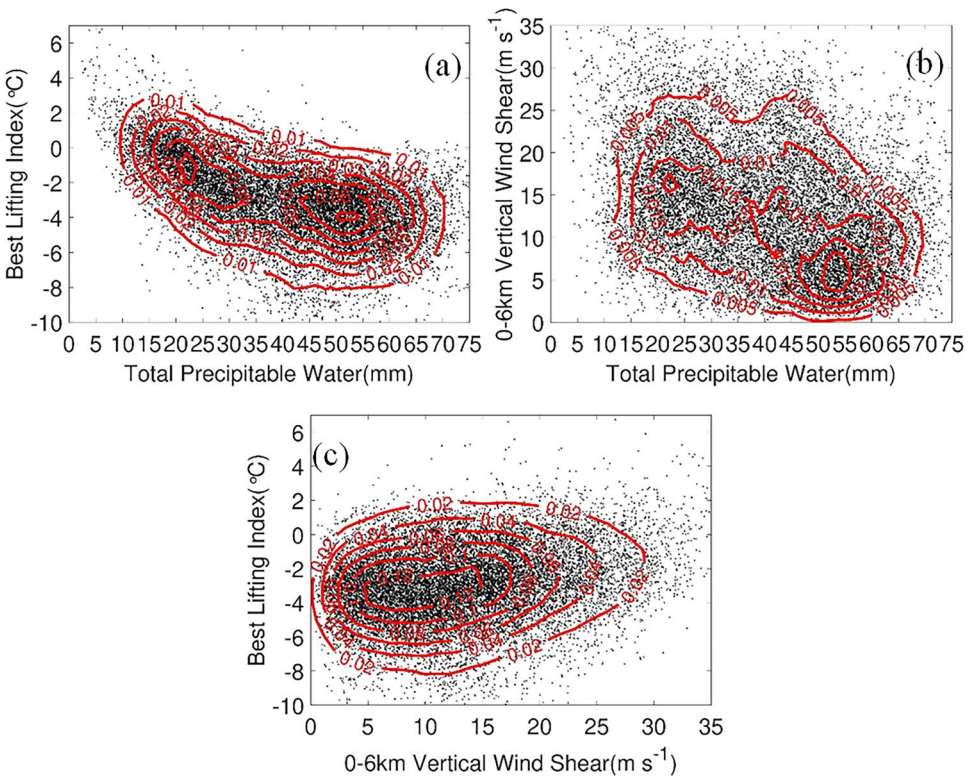

Fig. 2 The scatter plots and kernel density estimation (KDE) of **a** TPW-MULI, **b** TWP-SHR6, and **c** MULI-SHR6 for studied THWs

characteristics (Fig. 3). The annual cycle of the percentage of dry and wet THWs shows the earliest THWs were dominated by dry THWs (Fig. 3a). Dry THWs accounted for 100% in early March and then decreased gradually to about 50% in early April. In August, the percentage of dry THW decreased to about 20% but soon increased to more than 80% in September. The wet THWs show opposite changing trends compared with dry THWs. There are two periods with the largest differences, one in mid-June and one in mid-August. The annual variation of the percentage of dry and wet THWs seems in good consistent with the variation of monsoon (Zhao et al. 2019). However, the dry and wet THWs have similar daily cycle characteristics (Fig. 3b). The afternoon to evening at the local time is the main occurrence period (BJT, Beijing standard time). The peak is at 5 p.m. The total proportion of dry and wet THWs from 2 to 9 p.m. (BJT) is 69.3% and 66.8%, respectively. A variation seems highly related to solar radiation (Amber and O'Donovan 2018).

5.2 Characteristics of pre-convection environmental conditions

5.2.1 Characteristics of TPW

TPW is the integration of the specific humidity from the ground to about 200 hPa. The TPW for total THWs range from 15 to 65 mm with a mean of about 40 mm (Fig. 4a). If divided with the TPW of 38 mm, the TPW range for dry THWs is between 12 and 38 mm, while that for wet THWs is between 38 and 68 mm. The corresponding relative frequency of TPW for total THWs indicates a wave valley at about 40 mm (Fig. 4b). The detailed characteristics cannot be delivered by the box-and-whisker plots.

The relative frequencies display more details about the distribution of TPW. Relative frequencies of dry and wet THWs also show a TPW of 38 mm as the threshold is reasonable (Fig. 4b). The 38-mm TPW threshold is almost the lowest point between the two peaks. With the 38-mm TPW as a threshold, the two peaks of the relative frequency of total THWs are separated into two with the means of TPW for dry and wet THWs are 25 and 55 mm, respectively (Fig. 4b). The two values are much close to the central values displayed in Fig. 2.

5.2.2 Characteristics of saturation conditions

Lower relative humidity (RH) indicating intrusion at middle levels is the key feature of many THWs. The box-and-whisker plots of RH_{200} show the range for dry and wet THWs is much different (Fig. 5a). The relative frequency of dry THWs shows the portion decreases as the saturation of RH_{200} increases. The peak for dry THWs is around 10%

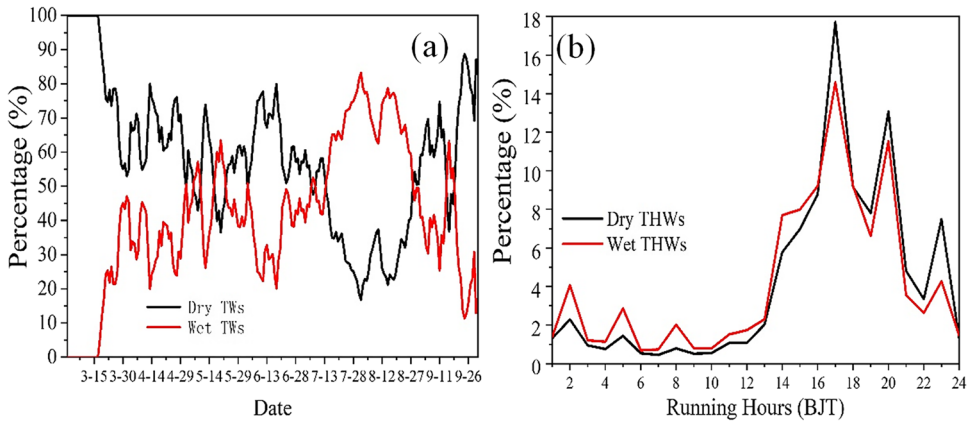

Fig. 3 The **a** yearly cycle and **b** daily cycle of the percentage of dry and wet THWs

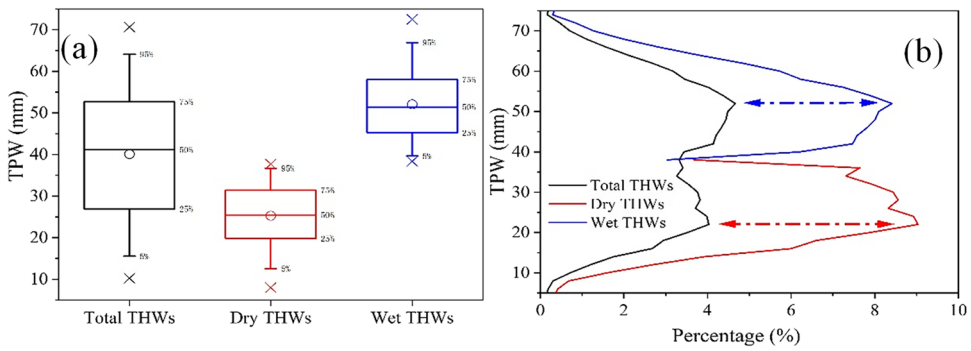

Fig. 4 The distribution of **a** box-and-whisker plots and **b** the relative frequency of TPW for total dry and wet THWs. The circles indicate the mean TPW while the crosses at the upper and the lower represent the 99th and the 1st percentiles, respectively

with a portion of about 10%. The RH_{200} for wet THWs is more evenly distributed except for a small peak for those higher than 90%. Both the box-and-whisker plots and relative frequencies of RH_{300} for dry and wet THWs are much the same (Fig. 5b). Except for those less than 10% and those greater than 90%, the difference of relative frequency at different RH is also small.

The box-and-whisker plots of RH_{500} for dry and wet THWs are also much the same. However, the relative frequencies show a small difference (Fig. 5c). A 40% RH_{500} is a threshold. For those greater than the threshold the relative frequency of wet THWs for the same RH_{500} is a little higher than that for dry THWs. For those less than the threshold the relative frequency of wet THWs for the same RH_{500} is a little less than that for dry THWs. The same characteristics can be seen for RH at lower pressure levels but with different RH thresholds. The difference can be revealed by both the box-and-whisker plots and relative frequencies. The box-and-whisker plots of RH_{700} show the favorable range for dry THWs is between 30 and 90%, but for wet THWs is between 40 and 90% (Fig. 5d). The relative frequencies show that a portion of wet THWs with an RH_{700} of about 70%. The

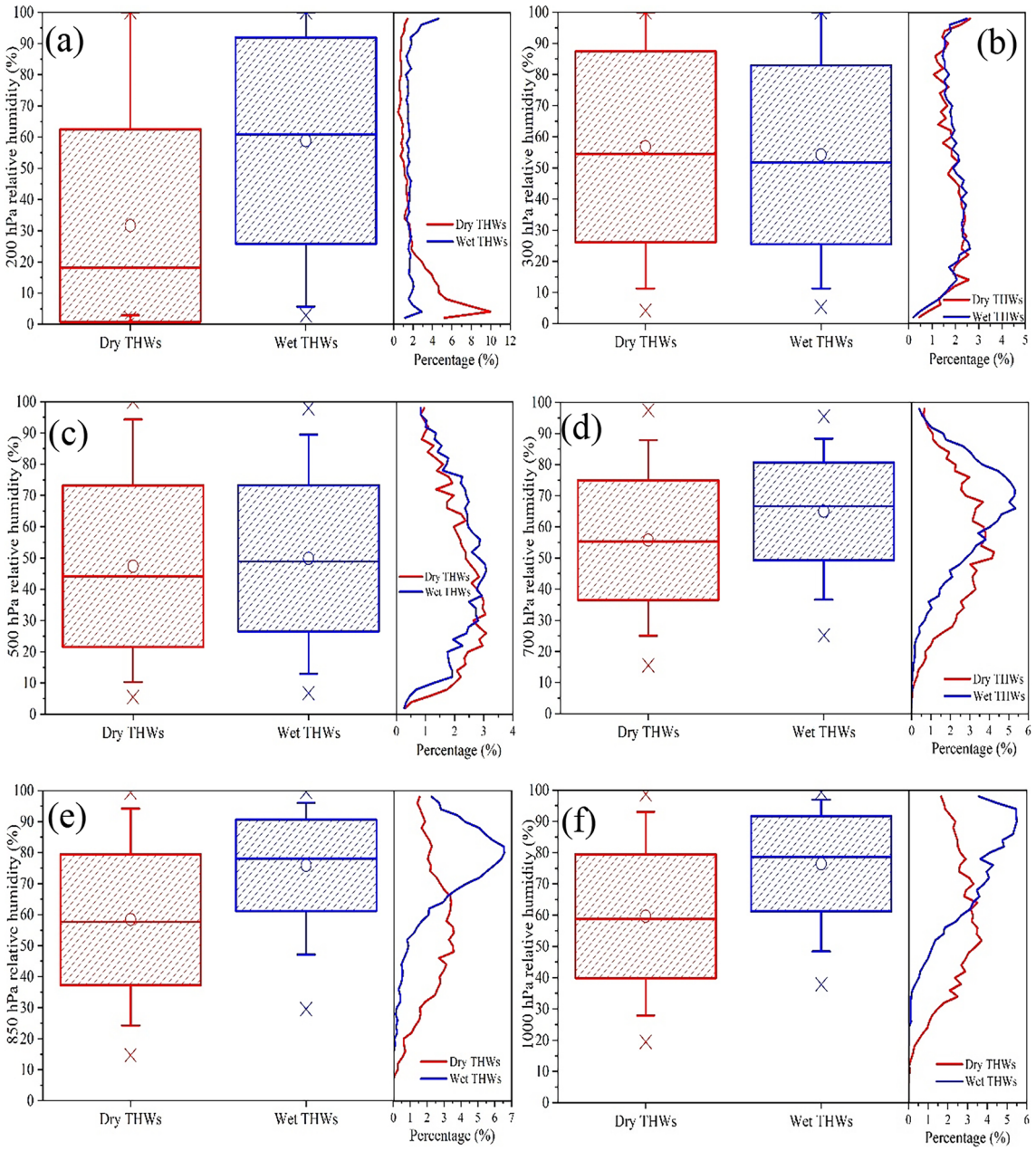

Fig. 5 Same as Fig. 4a, but for **a** RH_{200}, **b** RH_{300}, **c** RH_{500}, **d** RH_{700}, **e** RH_{850}, and **f** RH_{1000}

maximum percentage is around 5%. Only a small part of wet THWs occurred with the RH_{700} less than 30%. But for wet THWs, the peak point is 50%, and the maximum percentage is about 4%. Wet THWs have more saturated 700 hPa RH environmental conditions compared with dry THWs. Furthermore, wet THWs have a more concentrated distribution compared with dry THWs. The characteristics are also revealed by RH_{850} (Fig. 5e) and RH_{1000} (Fig. 5f) but with differences in details especially for wet THWs. The main range of RH_{850} for wet THWs is between 50 and 90% while for dry THWs is between 20 and 90%. The maximum relative frequency for dry and wet THWs is about 4% and 7%, respectively, with the corresponding RH_{850} of about 60% and 80%. The dry THWs have a maximum relative frequency of about 4% for RH_{1000} at 50% while the maximum relative frequency for wet THWs is about 6% at 90%.

The main difference in saturation conditions for dry and wet THWs is at the middle to lower levels of the troposphere. Dry THWs can occur at a saturation range between 10 and 100% while wet THWs usually have higher saturation conditions. The difference at RH_{200} could be caused by that 200 hPa is already in the stratosphere. This could be illustrated by the representative soundings given below. However, except for saturation conditions, instability also plays an important role.

5.2.3 Characteristics of instability conditions

The stability properties of the atmospheric environment are important in knowing whether severe convective weather can occur or not. A comparative analysis of multiple large-scale environmental thermal representative parameters is given to reveal the unique instability characteristics of wet and dry THWs environments.

The distribution of the most unstable lifted index (MULI) shows that almost all the wet THWs occur within negative MULI (Fig. 6a). The mean MULI is − 4 °C. However, there are about a quarter of dry THWs that occur with a positive MULI. The relative frequency of dry and wet THWs depicts the details. The peaks of the relative frequency of dry and wet THWs are − 1 and − 3 °C, respectively. The best convective available potential energy (MUCAPE) shows similar characteristics compared to MULI (Fig. 6b). Most wet THWs occur with a certain amount of MUCAPE. The main range of MUCAPE is between 500 and 2000 $J{\cdot}kg^{-1}$ with a mean value of about 1500 $J{\cdot}kg^{-1}$. However, there are about a quarter of dry THWs happened without any MUCAPE. This is the same as MULI shows but not consistent with a common understanding. It seems that MULI or MUCAPE is the necessary component of wet THWs, but not for dry THWs. Kuchera and Parker (2006) studied the environmental characteristics of non-tornado-caused catastrophic thunderstorms in the USA and found that lapse rates aloft were moderately discriminating between damaging and non-damaging convective wind environments. The performance of temperature difference (DT85) and lapse rate between 850 and 500 hPa (TLR85) are then investigated.

DT85 and TLR85 are more physically meaningful indicators of dry THWs compared to MULI and MUCAPE. The main range of DT85 for wet THWs is between 22 and 30 °C while for dry THWs is between 23 and 35 °C (Fig. 6c). The range for wet THWs is much smaller than that for dry THWs. The corresponding ranges of TLR85 for dry and wet THWs are 5.5 ~ 8.4 and 5.0 ~ 7.0 $°C{\cdot}km^{-1}$ (Fig. 6d), respectively. The peaks of TLR85 for dry and wet THWs are 7.0 and 6.0 $°C{\cdot}km^{-1}$, respectively. For reference, the wet adiabatic lapse rate is about 5.5 $°C{\cdot}km^{-1}$, the dry adiabatic lapse rate is about 9.8 $°C{\cdot}km^{-1}$, and the temperature lapse of standard atmosphere between above the ground and 6-km altitude is about 6.5 $°C{\cdot}km^{-1}$. A temperature lapse rate greater than 7.0 $°C{\cdot}km^{-1}$ can be considered strong. Figure 6d shows more than three-quarters of wet THWs have the TLR85 less than 6.5 $°C{\cdot}km^{-1}$. This may be related to the high moisture content (Fig. 5) and high saturation (Fig. 6) environments for wet THWs. More than half of dry THWs occur with TLR85 higher than 7.0 $°C{\cdot}km^{-1}$ (Fig. 6d). Seeley and Romps (2015) documented that undilute buoyancy increases monotonically throughout the troposphere with decreasing relative humidity with a so-called "zero-buoyancy" theory test. However, the actual is that if we keep the Q constant the decrease of RH could lead to the uplift of lifting condensation level (LCL) which leads to smaller MUCAPE (Chen et al. 2020). The mean LCL for dry THWs is higher than that for wet THWs (Fig. 7) but not significant enough.

The difference of T850 for dry and wet THWs is not as significant as T500 (Fig. 6e, f). The range of the box of T850 for dry THWs is 14 ~ 21 °C, and the corresponding range for wet THWs is 19 ~ 22 °C. The concentration of T850 for wet THWs is much higher than that for dry THWs (Fig. 6e). However, the range of T500 for dry THWs is between − 2 and − 25 °C with a mean of about − 12 °C. The range for wet THWs is between 0 and − 10 °C with a mean of about − 4 °C (Fig. 6f). Only about 50% of T500 for wet THWs overlapped with that for dry THWs. The T500 for dry THWs is much lower than that for wet THWs. The difference of DT85 and TRL85 for dry and wet THWs is caused by the lower T500 rather than the higher T850. This indicates that more attention should be paid to the severe decrease of T500 in predicting dry THWs.

The problem of instability is intricate (Schultz et al. 2000) and out of the scope of this study. A general explanation is that both MUCAPE and temperature lapse rate can indicate atmosphere instability. MUCAPE, as a kind of CAPE, in a physical sense is loosely the vertically integrated buoyancy of an adiabatically lifted sub-cloud atmosphere. MULI

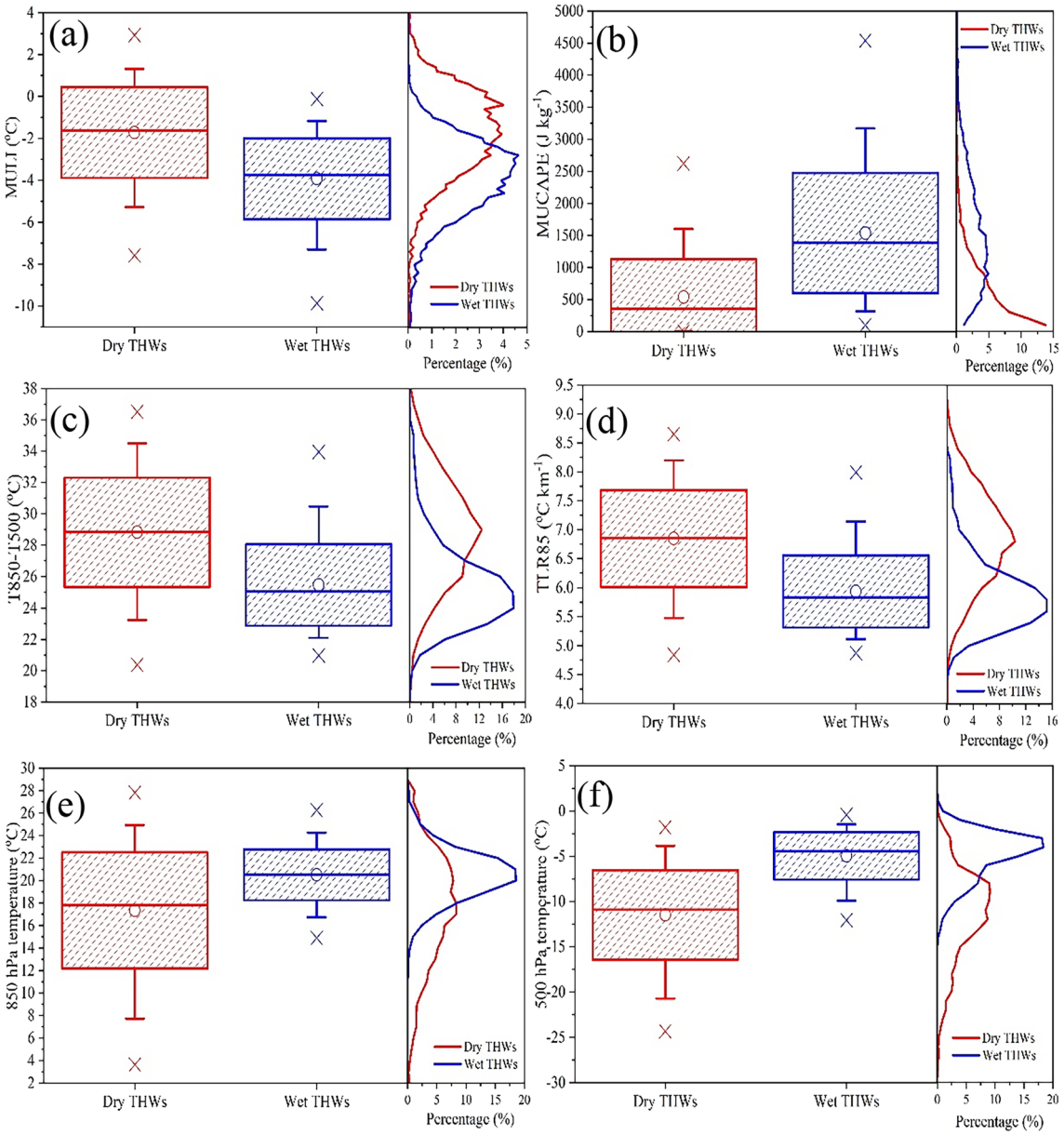

Fig. 6 Same as Fig. 4a, but for **a** MULI, **b** MUCAPE, **c** DT85, **d** TLR85, **e** T_{850}, and **f** T_{500}

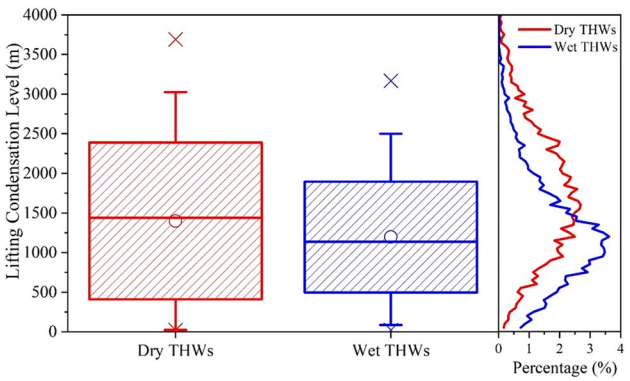

Fig. 7 Same as Fig. 4a, but for LCL

is to a certain extent another display of MUCAPE. Both MULI and MUCAPE have good performance under environments with a large amount of moisture content and can help estimate the possible strength of convection. The study about temperature lapse rate is more detailed (Bryan and Fritsch 2000; Nakamura 2011) but could not help estimate the strength of possible convection. However, the MULI and MUCAPE are not suitable for the recognition of dry THWs environments that usually have limited moisture content as displayed in this study. The temperature lapse rate performs much better. This provides a different view on using the different instability indicators under synoptic environments for dry and wet THWs, respectively.

5.2.4 Characteristics of low-level divergence and vertical wind shear conditions

Both wet and dry THWs occur in favorable low-level dynamic lifting environments. Detailed analyses show that the difference between dry and wet THWs for the DIV_{925} and DIV_{850} is much smaller (Fig. 8a, b). The mean value of DIV_{925} and DIV_{850} for both dry and wet THWs are both around 0.0 s^{-1}. This could be caused by the truth that instability and moisture indicating the status of the environmental conditions can last for relatively a longer period. The environmental condition of instability and moisture would be destroyed by the triggering of convection or other mechanisms. However, the influence of dynamic lifting lasts relatively short. Convections will be initiated when the environment with a certain amount of moisture and instability encounters favorable dynamic lifting, such as the fronts or the convergence lines. The closest hour before the exact time of each of the THWs could not be the moment the THW is happening.

Vertical wind shear (SHR) is another important factor for severe convection. The box-and-whisker plots and distribution of 0 ~ 1 km SHR (SHR_1) for dry and wet THWs are much the same indicating almost the same low-level wind shear conditions (Fig. 8c). Comparatively, the vertical wind shear of 0 ~ 6 km SHR (SHR_6) performs better than SHR_1 on distinguishing dry and wet THWs. The SHR_6 for dry THWs is much stronger than that for wet THWs. About 50% of dry THWs concentrate within 10 ~ 20 $m{\cdot}s^{-1}$ as the box shows (Fig. 8d). The corresponding range for wet THWs is 5 ~ 15 $m{\cdot}s^{-1}$. The mean values for dry and wet THWs are 15 and 11 $m{\cdot}s^{-1}$, respectively. The relative frequency provides more details but is much the same as the box-and-whisker plots show.

5.2.5 Representative soundings

The representative soundings provide overall characteristics of the environment conditions (Fig. 9). The representative soundings are obtained with the representative temperatures and representative dew point temperatures of the 27 pressure levels. The representative dew point temperatures are calculated with the representative specific humidity and temperatures. The representative soundings are obtained as follows: the first is to obtain the representative temperature and relative humidity of 27 pressure levels. The representative value for a specific pressure level is determined by checking the distribution of relative frequency of temperature as shown in Fig. 6e, f, and those for relative humidity are shown in Fig. 5. The value related to the maximum relative frequency is picked as the representative value. Second is the calculation of representative dew temperature. The representative dew temperature is calculated with the representative temperature and relative humidity as no dew temperature data is directly available. The third is the obtaining of the soundings. The soundings obtained with the representative values are more representative than the averaged sounding and represent the most likely probability of occurrence of dry and wet THWs.

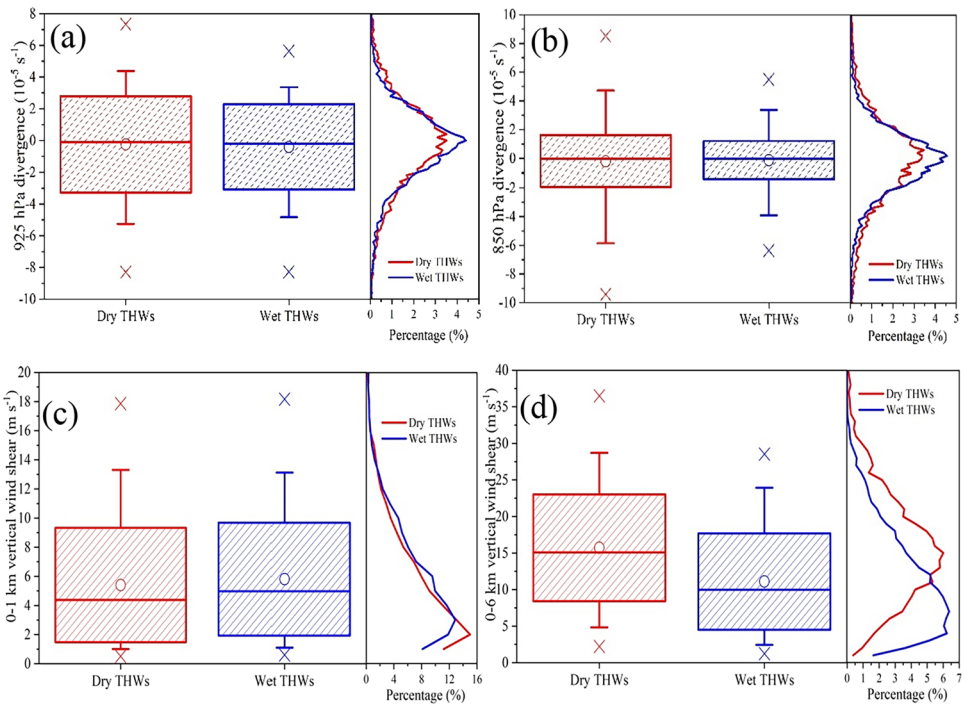

Fig. 8 Same as Fig. 4a, but for **a** DIV_{925}, **b** DIV_{850}, **c** SHR_1, and **d** SHR_6

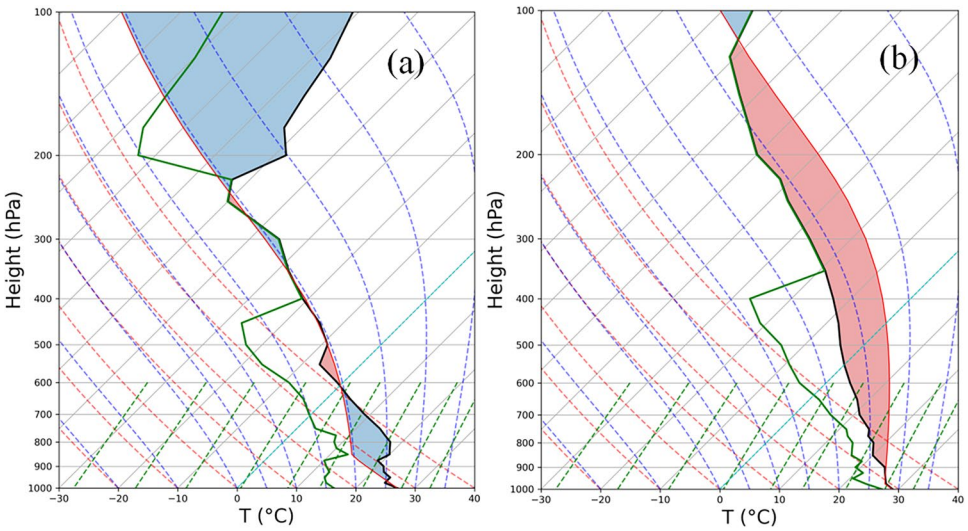

Fig. 9 The representative sounding for **a** dry and **b** wet THWs

The representative soundings of dry and wet THWs show the comprehensive characteristics of the environmental conditions. The dramatic difference in representative soundings could be the type of CAPE as shown in Fig. 9. The thin and short CAPE for dry THW is between 600 and 400 hPa (Fig. 9a). The CAPE for wet THW is fat and tall and stretches upwards to about 100 hPa with the bottom at about 900 hPa (Fig. 9b). The different CAPE shapes are determined by the profile of temperature and dew point temperature. The near-surface temperature for dry THWs is smaller than that for wet THWs, and there is a temperature reversal at 850 hPa for dry THWs (Fig. 9a). The sounding reflects the general status of the environmental conditions. The soundings also show low saturation areas at both middle-lower levels and upper levels for dry THWs, but only low saturation areas at the middle-lower levels for wet THWs. The middle-lower low saturation areas could be caused by the dry intrusions. However, the upper low saturation area in the sounding for dry THWs is undoubtedly caused by the stratosphere as the tropopause indicates. The tropopause in the representative sounding for dry THWs is at about 200 hPa. Meanwhile, the tropopause in the representative sounding for wet THWs is higher than 100 hPa. Lower tropopause always means a lower temperature at the same pressure level. The lower tropopause for dry THWs can partly explain the better performance of DT85 and TLR85 in distinguishing from wet THWs. Studies show that specific patterns of tropopause such as tropopause folds can lead to strong surface wind by reducing the stability beneath the fold (Griffiths et al. 2000). The midlatitude areas where the studied area is located in usually experience tropopause folds though the frequency of tropopause folds is significantly smaller in the summer than in the other seasons (Elbern et al. 1998). The tropopause influences both dry and wet THWs, but mechanisms should be further explored.

6 Conclusions and discussions

By using SWRs, and the CLDN lightning data, the quality-controlled THWs are obtained. With the ERA5 parameters from March 1 to September 30, 2010–2019, the dry and wet THWs are divided by TPW by adopting the KDE. The climatological characteristics of dry and wet THWs and environmental conditions are then investigated. The main findings are summarized as follows:

1) TPW is an effective indicator of environmental conditions favorable for dry or wet THWs. A TPW of 38 mm can be used as the threshold for distinguishing dry and wet THW environments.
2) The THWs over North China are mainly composed of dry ones, while THWs over South China are mainly composed of wet ones. West of Hebei has high frequencies for both dry and wet THWs. THWs over Yun'nan are mainly the dry ones. THWs during the deep summer seasons are dominated by wet THWs while other seasons are dominated by dry ones.
3) Wet THWs can be well characterized by MULI and MUCAPE while dry THWs can be well characterized by higher temperature differences or temperature lapse rates caused by lower 500 hPa temperature. Dry THWs occur under a relatively high SHR_6 environment.
4) Representative soundings show the CAPE for dry THWs is thin and small while for wet THWs is fat and tall. The middle and lower low saturation areas are the common features of dry and wet THWs.

The THWs environment in eastern China is much different from that of other nations (Kuchera and Parker 2006; Taszarek et al. 2020). It might be caused by different definitions of damaging wind. The damaging wind described by Kuchera and

Parker (2006) is to a great extent the wet environment convective wind as they are long-lived, widespread ones. Observations show that many of the dry THWs in China are usually produced by isolated convections with a relatively short lifetime (Yang and Sun 2018). Though a TPW of 38 mm can distinguish the KDE in the scatter plots, the actual environmental conditions for THWs could be much more complex than we have known. This study provides a comprehensive understanding of the climatology and environmental conditions of dry and wet THWs over eastern China. How the physical processes within THWs-producing MCS are affected by different TPW amounts is still unknown and needs further to be explored.

Acknowledgements Dr. Zi Mai of the National Meteorological Center helped with the production of Fig. 9. We are grateful to the reviewers and the editors for their valuable comments.

Author contribution FT, JS, and KX designed the experiment, conducted the analysis, and wrote the initial manuscript. FT, JS, and XZ contributed to the idea. SH and BY processed the ERA5 data. QW executed the quality control of observations. LX and KX improved the manuscript. All authors reviewed the manuscript.

Funding This research was jointly supported by the National Natural Science Foundation of China (U2142202), the Key R&D Program of Xizang Autonomous Region (XZ202101ZY0004G), the National Key R&D Program of China (2022YFC3004104), and the Key Innovation Team of China Meteorological Administration (CMA2022ZD07).

Data availability The severe weather reports, cloud-to-ground lightning data, and surface routine observations used in this study were obtained from the National Meteorological Information Center at http://data.cma.cn/ (accessed on 21 Nov. 2022). The ERA5 dataset was available at https://cds.climate.copernicus.eu/cdsapp#!/dataset/reanalysis-era5-pressure-levels?tab=form (accessed on 21 Nov. 2022).

Declarations

Conflict of interest The authors declare no competing interests.

References

Amber I, O'Donovan TS (2018) Natural convection induced by the absorption of solar radiation: a review. Renew Sustain Energy Rev 82:3526–3545. https://doi.org/10.1016/j.rser.2017.10.106

Atkins NT, Wakimoto RM (1991) Wet microburst activity over the Southeastern United States: implications for forecasting. Wea Forecasting 6(4):470–482. https://doi.org/10.1175/1520-0434(1991)006%3c0470:WMAOTS%3e2.0.CO;2

Atkins NT, Laurent MS (2009a) Bow echo mesovortices Part I.: progresses that influence their damaging potential. Mon Wea Rev 137(5):1497–1513. https://doi.org/10.1175/2008MWR2649.1

Atkins NT, Laurent MS (2009b) Bow echo mesovortices Part II.: their genesis. Mon Wea Rev 137(5):1514–1532. https://doi.org/10.1175/2008MWR2650.1

Atkins NT, Bouchard CS, Przybylinski RW, Trapp RJ, Schmocker G (2005) Damaging surface wind mechanisms within the 10 June 2003 Saint Louis bow echo during BAMEX. Mon Wea Rev 133(8):2275–2296. https://doi.org/10.1175/MWR2973.1

Bluestein HB, Jain MH (1985) Formation of mesoscale lines of precipitation: severe squall lines in Oklahoma during the spring. J Atmos Sci 42(16):1711–1732. https://doi.org/10.1175/1520-0469(1985)042%3c1711:FOMLOP%3e2.0.CO;2

Brown A, Dowdy A (2021) Severe convective wind environments and future projected changes in Australis. J. Geophysic Res Atmos 126(16):e2021JD034633. https://doi.org/10.1029/2021JD034633

Bryan GH, Fritsch JM (2000) Moist absolute instability: the sixth static stability state. Bull Amer Meteor Soc 81(6):1207–1230. https://doi.org/10.1175/1520-0477(2000)081%3c1287:MAITSS%3e2.3.CO;2

Chen J, Dai AG, Zhang YC, Rasmussen KL (2020) Changes in convective available potential energy and convective inhibition under global warming. J Climate 33(6):2025–2050. https://doi.org/10.1175/JCLI-D-19-0461.1

Doswell CA III (2001) Severe convective storms – An overview. In: Doswell CA (ed) Severe Convective Storms. Springer, New York, pp 1–26

Duda JD, Gallus W Jr (2010) Spring and summer Midwestern severe weather reports in supercells compared to other morphologies. Wea Forecasting 25(1):190–206. https://doi.org/10.1175/2009WAF2222338.1

Elbern H, Hendricks J, Ebel A (1998) A climatology of tropopause folds by global analyses. Theor Appl Climatol 59:181–200. https://doi.org/10.1007/s007040050023

Fan LM, Yu XD (2013) Characteristic analyses on environmental parameters in short-term severe convective weather in China (in Chinese). Plateau Meteor 32(1):156–165. https://doi.org/10.7522/j.issn.1000-0534.2012.00016

Fei HY, Wang XM, Zhou XG, Yu XD (2016) Climatic characteristics and environmental parameters of severe thunderstorm gales in China (in Chinese). Meteor Mon 42(12):1513–1521. https://doi.org/10.7519/j.issn.1000-0526.2016.12.009

Fujita TT (1978) Manual of downburst identification for Project NIMROD. In: Satellite and Mesometeorology Research Paper, vol 156. Dept. of Geophysical Sciences, University of Chicago, Chicago, IL, p 104

Gallus WA Jr, Snook NA, Johnson EV (2008) Spring and summer severe weather reports over the Midwest as a function of convective mode: a preliminary study. Wea Forecasting 23(1):101–113. https://doi.org/10.1175/2007WAF2006120.1

Galway JG (1956) The lifted index as a predictor of latent instability. Bull Amer Meteor Soc 37(10):528–529. https://doi.org/10.1175/1520-0477-37.10.528

Griffiths M, Thorpe AJ, Browning KA (2000) Convective destabilization by a tropopause fold diagnosed using potential-vorticity inversion. Q J R Meteorol Soc 126:125–144. https://doi.org/10.1002/qj.49712656207

Hersbach H et al (2020) The ERA5 global reanalysis. Quart J Royal Meteorol 146(730):1999–2049. https://doi.org/10.1002/qj.3803

Houze RA, Rutledge SA, Biggerstaff MI, Smull BF (1989) Interpretation of doppler weather radar displays in midlatitude mesoscale convective systems. Bull Amer Meteor Soc 70(6):608–619. https://doi.org/10.1175/1520-0477(1989)070%3c0608:IODWRD%3e2.0.CO;2

James RP, Markowski PM, Fritsch JM (2006) Bow echo sensitivity to ambient moisture and cold pool strength. Mon Wea Rev 134(3):950–964. https://doi.org/10.1175/MWR3109.1

Jirak IL, Cotton WR, Mcanelly RL (2003) Satellite and radar survey of mesoscale convective system development. Mon Wea Rev 131(10):2428–2448. https://doi.org/10.1175/1520-0493(2003)131%3c2428:SARSOM%3e2.0.CO;2

Klimowski BA, Bunkers MJ, Hjelmfelt MR, Covert JN (2003) Severe convective windstorms over the Northern High Plains of the United States. Wea Forecasting 18(3):502–519. https://doi.org/10.1175/1520-0434(2003)18%3c502:SCWOTN%3e2.0.CO;2

Klimowski BA, Hjelmfelt MR, Bunkers MJ (2004) Radar observations of the early evolution of bow echoes. Weather Forecast 19(4):727–734. https://doi.org/10.1175/1520-0434(2004)019%3c0727:ROOTEE%3e2.0.CO;2

Kuchera EL, Parker MD (2006) Severe Convective Wind Environments Wea Forecasting 21(4):595–612. https://doi.org/10.1175/WAF931.1

Ma SP, Wang XM, Yu XD (2019) Environmental parameter characteristics of severe wind with extreme thunderstorm (in Chinese). J Appl Meteor Sci 30(3):292–301. https://doi.org/10.11898/1001-7313.20190304

Ma RY, Sun JH, Yang X (2021) An eight-year climatology of the warm-season severe thunderstorm environments over North China. Atmos Res 254(2021):105519. https://doi.org/10.1016/j.atmosres.2021.105519

Meng ZY, Yan DC, Zhang YJ (2013) General features of squall lines in East China. Mon Wea Rev 141(5):1629–1647. https://doi.org/10.1175/MWR-D-12-00208.1

Meng ZY, Yao D, Bai LQ, Zheng YG, Xue M, Zhang XL, Zhao K, Tian FY, Wang MJ (2016) Wind estimation around the shipwreck of Oriental Star based on field damage surveys and radar observations. Sci Bull 61(4):330–337. https://doi.org/10.1007/s11434-016-1005-2

Mohr S, Kunz M, Richter A, Ruck B (2017) Statistical characteristics of convective wind gusts in Germany. Nat Hazards Earth Sys Sci 17(6):957–969. https://doi.org/10.5194/nhess-17-957-2017

Moller AR, Doswell CA III, Foster MP, Woodall GR (1994) The operational recognition of supercell thunderstorm environments and storm structures. Wea Forecasting 9(3):327–347. https://doi.org/10.1175/1520-0434(1994)009%3c0327:TOROST%3e2.0.CO;2

Nakamura K (2011) Reconsideration of conditional instability – static stability of a saturated air parcel in an unsaturated environment. J Meteor Soc Japan 89(5):495–516. https://doi.org/10.2151/jmsj.2011-506

Pacey GP, Schultz DM, Garcia-Carreras L (2021) Severe convective windstorms in Europe: climatology, preconvective environments, and convective mode. Wea Forecasting 36(1):237–252. https://doi.org/10.1175/WAF-D-20-0075.1

Park MD, Johnson RH (2000) Organizational modes of midlatitude mesoscale convective systems. Mon Wea Rev 128(10):3413–3436. https://doi.org/10.1175/1520-0493(2001)129%3c3413:OMOMMC%3e2.0.CO;2

Parker MD, Johnson RH (2000) Organizational modes of midlatitude mesoscale convective systems. Mon Wea Rev 128(10):3413–3436. https://doi.org/10.1175/1520-0493(2001)129%3c3413:OMOMMC%3e2.0.CO;2

Przybylinski RW (1995) The bow echo: Observations, numerical simulations, and severe weather detection methods. Wea Forecasting 10(2):203–218. https://doi.org/10.1175/1520-0434(1995)010%3c0203:TBEONS%3e2.0.CO;2

Roberts RD, Wilson JW (1989) A proposed microburst nowcasting procedure using single-Doppler radar. J Appl Meteor 28(4):285–303. https://doi.org/10.1175/1520-0450(1989)028%3c0285:APMNPU%3e2.0.CO;2

Schoen JM, Ashley WS (2011) A climatology of fatal convective wind events by storm type. Wea Forecasting 26(1):109–121. https://doi.org/10.1175/2010WAF2222428.1

Schultz DM, Schumacher PN, Doswell CA III (2000) The intricacies of instabilities. Mon Wea Rev 128(12):4143–4148. https://doi.org/10.1175/1520-0493(2000)129%3c4143:TIOI%3e2.0.CO;2

Seeley JT, Romps DM (2015) Why does tropical convective available potential energy (CAPE) increase with warming? Geophy Res Lett 42(23):10429–10437. https://doi.org/10.1002/2015GL066199

Smith BT, Thompson RL, Grams JS, Broyles C, Brooks HE (2012) Convective modes for significant severe thunderstorms in the contiguous United States Part I.: storm classification and climatology. Wea. Forecasting 27(5):1114–1135

Smith BT, Castellanos TE, Winters AC, Mead CM, Dean AR, Thompson RL (2013) Measured severe convective wind climatology and associated convective modes of thunderstorms in the contiguous United States, 2003–09. Wea Forecasting 28(1):229–236. https://doi.org/10.1175/WAF-D-12-00096.1

Smull BF, Houze RA (1985) A midlatitude squall line with a trailing region of stratiform rain: radar and satellite observations. Mon Wea Rev 113(1):117–133. https://doi.org/10.1175/1520-0493(1985)113%3c0117:AMSLWA%3e2.0.CO;2

Sun JH, Zheng LL, Zhao SX (2014) Impact of moisture on the organizational mode and intensity of squall lines determined through numerical experiments (in Chinese). Chinese J Atmos Sci 38(4):742–755. https://doi.org/10.3878/j.issn.1006-9895.2013.13187

Tao SY (1980) Rainstorms in China (in Chinese). Science Press, Beijing, pp 5–7

Taszarek M, Allen JT, Púčik T, Hoogewind KA, Brooks HE (2020) Severe convective storms across Europe and the United States. Part II: ERA5 environments associated with lightning, large hail, severe wind, and tornadoes. J Climate 33(23):10263–10286. https://doi.org/10.1175/JCLI-D-20-0346.1

Tian FY, Zheng YG, Zhang T, Mao DY, Tang WY, Zhou QL, Sun JH, Zhao SX (2015) Sensitivity analysis of short-duration heavy rainfall related diagnostic parameters with point-area verification (in Chinese). J Appl Meteor Sci 26(4):385–396. https://doi.org/10.11898/1001-7313.20150401

Tian FY, Zheng YG, Zhang T, Zhang XL, Mao DY, Sun JH, Zhao SX (2015b) Statistical characteristics of environmental parameters for warm season short-duration heavy rainfall over central and eastern China. J Meteor Res 29(3):370–384. https://doi.org/10.1007/s13351-014-4119-y

Tian FY, Zhang XL, Cao YC, Sun JH, Zheng YG, Yang XL, Han XQ, Mai Z (2022) Baseline climatology of environmental parameters for three severe convective weather phenomena in middle-low areas of China (in Chinese). Plateau Meteor 41(6):1446–1459. https://doi.org/10.7522/j.issn.1000-0534.2021.00108

Trapp RJ, Weisman ML (2003) Low-level mesovortices within squall lines and bow echoes Part II: their genesis and implications. Mon Wea Rev 131(11):2804–2823. https://doi.org/10.1175/1520-0493(2003)131%3c2804:LMWSLA%3e2.0.CO;2

Wakimoto RM (1985) Forecasting dry microburst activity over the high plains. Mon Wea Rev 113(7):1131–1143. https://doi.org/10.1175/1520-0493(1985)113%3c1131:FDMAOT%3e2.0.CO;2

Wakimoto RM, Murphey HV, Nester A, Jorgensen DP, Atkins N (2006a) High winds generated by bow echoes Part I: overview of the Omaba bow echo 5 July 2003 storm during BAMEX. Mon Wea Rev 134(10):2793–2812. https://doi.org/10.1175/MWR3215.1

Wakimoto RM, Murphey HV, Davis CA, Atkins N (2006b) High winds generated by bow echoes Part II: the relationship between the mesovortices and damaging straight-line winds. Mon. Wea. Rev. 134(10):2813–2829. https://doi.org/10.1175/MWR3216.1

Wang DH, Li XF, Tao WK, Wan Y (2009) Effects of vertical wind shear on convective development during a landfall of severe

tropical storm Bilis (2006). Atmos Res 94(2):270–275. https://doi.org/10.1016/j.atmosres.2009.06.004

Wang XM, Yu XD, Zhou XG, Niu SZ (2012) Study on the formation and evolution of '6.3' damage wind (in Chinese). Plateau Meteor 31(2):504–514

Wang ZH, Chen P, Wang R, An ZY, Yang XY (2023) Performance of ERA5 data in retrieving precipitable water vapor over Hong Kong. Adv Space Res 71(10):4055–4071. https://doi.org/10.1016/j.asr.2022.12.059

Weisman ML (2001) Bow Echoes: A Tribute to T. T Fujita Bull Amer Meteor Soc 82(1):97–116. https://doi.org/10.1175/1520-0477(2001)082%3c0097:BEATTT%3e2.3.CO;2

Weisman ML, Klemp JB (1982) The dependence of numerically simulated convective storms on vertical wind shear and buoyancy. Mon Wea Rev 110(6):504–520. https://doi.org/10.1175/1520-0493(1982)110%3c0504:TDONSC%3e2.0.CO;2

Wheatley DM, Trapp RJ, Atkins NT (2006) Radar and damage analysis of severe bow echoes observed during BAMEX. Mon Wea Rev 134(3):791–806. https://doi.org/10.1175/MWR3100.1

Wolfson M, Klingle-Wilson D, Donovan M, Cullen J, Neilley D, Liepins M, Hallowell R, DiStefano J, Clark D, Isaminger M, Biron P, Forman B (1990) Characteristics of thunderstorm-generated low altitude wind shear: a survey based on nationwide Terminal Doppler Weather Radar testbed measurements. In: Proc. 29th IEEE Conf. on Decision and Control. Institute of Electrical and Electronics Engineers, Honolulu, HI, pp 682–688. https://doi.org/10.1109/CDC.1990.203681

Xu X, Xue M, Wang Y (2015) The genesis of mesovortices within a real-data simulation of a bow echo system. J Atmos Sci 72(5):1963–1986. https://doi.org/10.1175/JAS-D-14-0209.1

Yang XL, Sun JH (2018) Organized modes of severe wind-producing convective systems over north China. Adv Atmos Sci 35(5):540–549. https://doi.org/10.1007/s00376-017-7114-2

Yang XL, Sun JH, Lu R, Zhang X (2017a) Environmental characteristics of severe convective wind over south China (in Chinese). Meteor Mon 43(7):769–780. https://doi.org/10.7519/j.issn.1000-0526.2017.07.001

Yang XL, Sun JH, Zheng YG (2017b) A 5-yr climatology of severe convective wind events over China. Wea Forecasting 32(4):1289–1299. https://doi.org/10.1175/WAF-D-16-0101.1

Zhang W, Zhang H, Lou Y, Cai Y, Cao Y, Zhou Y, Liu W (2019) On the suitability of ERA5 in hourly GPS precipitable water vapor retrieval over China. J Geodesy 93:1897–1909. https://doi.org/10.1007/s00190-019-01290-6

Zhao W, Chen SF, Chen W, Yao S, Nath D, Yu B (2019) Interannual variation of the rainy season withdrawal of the monsoon transitional zone in China. Cli Dyna 53:2031–2046. https://doi.org/10.1007/s00382-019-04762-9

Zheng LL, Sun JH (2013) Characteristics of synoptic and surface circulation of mesoscale convective systems in dry and moist environmental conditions (in Chinese). Chinese J Atmos Sci 37(4):891–904. https://doi.org/10.3878/j.issn.1006-9895.2012.12090

Zheng LL, Sun JH (2016) The impact of vertical wind shear on the intensity and organizational mode of mesoscale convective systems using numerical experiments (in Chinese). Chinese J Atmos Sci 40(2):324–340. https://doi.org/10.3878/j.issn.1006-9895.1505.14311

Zheng YG, Tian FY, Meng ZY, Xue M, Yao D, Bai LQ, Zhou XX, Mao X, Wang MJ (2016) Survey and multiscale characteristics of wind damage caused by convective storms in the surrounding area of the capsizing accident of cruise ship "Dongfangzhixing" (in Chinese). Meteor Mon 42(1):1–13. https://doi.org/10.7519/j.issn.1000-0526.2016.01.001